Imaging the dynamics of magma propagation using radiated seismic intensity

B. Taisne,[1] F. Brenguier,[1,2] N. M. Shapiro,[1] and V. Ferrazzini[2,3]

Received 3 November 2010; revised 14 January 2011; accepted 19 January 2011; published 22 February 2011.

[1] At shallow depth beneath the Earth's surface, magma propagates through strongly heterogeneous volcanic material. Inversion of buoyancy and/or solidification have strong impacts on the dynamics of propagation without any change of magma supply. In this paper, we study the spatial and time evolution of magma intrusions using induced seismicity. We propose a new method based on ratio analysis of estimates of radiated seismic intensities recorded at different stations during seismic swarms. By applying this method to the January 2010 Piton de la Fournaise volcano eruption, we image complex dike propagation dynamics which strongly differ from a model of constant velocity dike propagation. We provide a new method to image in real time the dynamics of dike propagation and to infer the position of eruptive fissures. **Citation:** Taisne, B., F. Brenguier, N. M. Shapiro, and V. Ferrazzini (2011), Imaging the dynamics of magma propagation using radiated seismic intensity, *Geophys. Res. Lett.*, *38*, L04304, doi:10.1029/2010GL046068.

1. Introduction

[2] Eruption precursory activity associated with volcanic unrest is currently recorded at many volcanological observatories around the world and mainly consists of seismicity and ground deformation monitoring. During magma propagation to the near-surface, the vicinity of the associated dike or sill is subjected to a large stress field perturbation [*Rubin and Gillard*, 1998], that will concentrate most of the induced seismicity (seismic swarms). Monitoring these seismic swarms is thus a potentially powerful technique to track magma movements but is not used to its full potential for several reasons. During swarms, seismic events are difficult to separate, so that one may not use the efficient location methods that have been devised for single earthquakes. Only those events with well identified P and S phases can be treated with current methods and a large part of the seismic signal is left unused. Consequently, the interpretation of the data in term of the dynamics of magma migration is difficult. Previously, few examples of migration of seismicity associated with magma movement have been imaged by geophyscial means [*Aoki et al.*, 1999; *Hayashi and Morita*, 2003; *Battaglia et al.*, 2005a]. However, precise analysis of seismicity (location and magnitude) requires post-processing and is therefore difficult to perform in real time.

[3] Here, we propose a simple and robust method to track magma movements using the ratio of the seismic intensities at different seismic stations radiated by the surroundings of the dike's tip. We apply this method to the January 2010 eruption of Piton de la Fournaise volcano (La Réunion island). As a result, we observe a complex dike propagation history which strongly differs from a model of constant velocity dike propagation. We thus provide a simple method to image dike propagation in near-real time and to predict the position of eruptive fissures.

2. Method

[4] Traditionally, seismic events are located using P or S wave travel time delays measured at different receivers. This approach finds its limits when it becomes difficult to measure accurate arrival times such as for example, during seismic swarms or in cases of low signal to noise ratio micro-seismicity. Here, we propose a method to automatically estimate the position at depth of a seismic source by using the differences in seismic amplitudes recorded at different sensors. This approach relies on the decay of seismic wave amplitude along the source-receiver travel path. In order to avoid the requirement of detecting P or S wave arrivals, we use an estimate of the average recorded seismic intensity over a time window much longer than the seismic wave travel time delays at different sensors (see section 3 for details). Following *Battaglia and Aki* [2003], we use a simple attenuation (equation (1)).

$$I_i = I_o \frac{e^{-Br_i}}{r_i^n}, \tag{1}$$

with,

$$B = \frac{\pi f}{Q\beta}, \tag{2}$$

where I_i is the seismic intensity (a measure of the amplitude of a velocity seismogram, see section 3) recorded at receiver i, r_i is the distance from the source, I_o is the source radiated seismic intensity, f is frequency, β is shear wave velocity and Q is the quality factor for attenuation. The index $n = 1$ for body waves and $n = 0.5$ for surface waves. For simplification we consider an isotropic medium with constant B.

[5] To avoid the estimate of the seismic intensity at the source (I_o), we choose to analyse the ratios of seismic intensities between sensors (equation (3), where t corresponds to time) rather than the true seismic intensities at different sensors.

$$\left.\frac{I_i}{I_j}\right|^t = \left(\frac{r_j^t}{r_i^t}\right)^n \exp\left[-B\left(r_i^t - r_j^t\right)\right]. \tag{3}$$

For the present purpose, and due to the fact that we use different pairs of stations, we will consider any temporal changes

[1]Department of Seismology, UMR 7154, Institut de Physique du Globe de Paris, Sorbonne Paris Cité, CNRS, Paris, France.
[2]Observatoire Volcanologique du Piton de la Fournaise, UMR 7154, Institut de Physique du Globe de Paris, Sorbonne Paris Cité, CNRS, La Plaine des Cafres, La Réunion.
[3]Géologie des Systèmes Volcaniques, UMR 7154, Institut de Physique du Globe de Paris, Sorbonne Paris Cité, CNRS, Paris, France.

0094-8276/11/2010GL046068

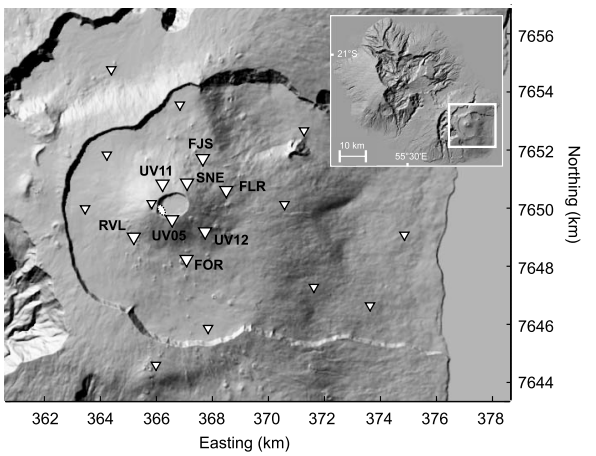

Figure 1. Location of Piton de la Fournaise volcano on La Réunion island (inset) and seismic station distribution (inverted triangles). Those used in this study are referred by their names on the map. The position of the January 2010 eruptive fissure is shown as a dashed circle.

as a result of the migration of the seismic source and therefore to the migration of the magma.

3. Example of Data Processing

[6] As an application of the proposed method, we focus on Piton de la Fournaise (PdF) volcano located on La Réunion island in the Indian ocean (Figure 1). It is a basaltic shield volcano which erupted more than 30 times between 2000 and 2010. Since 2009–2010, 15 broad-band seismic stations have been installed on the volcano as part of the Understanding Volcano project (UnderVolc), in addition to the existing seismic array.

[7] We analyse data from the 2010 January eruption. The selected eruption presents a seismic swarm that can be divided into two phases (Figures 2a and 2b). During the first phase, which lasted for about an hour, a high level of seismicity was recorded followed by a relatively quiet phase that directly preceded the onset of the eruption (indicated by continuous seismic tremor).

[8] As a first stage of data processing we correct the signal for the instrument responses to retrieve accurate values of ground motion velocity. Seismic signal amplitudes have also been corrected for site effects using the coda amplification factor method [*Aki and Ferrazzini*, 2000].

[9] Seismicity induced by magma migration has a relatively high frequency content compared to the back-ground noise. For this study we only consider a frequency range between 5Hz and 15Hz (relevant for volcano-tectonic events).

[10] We calculate the envelope of the signal using the norm of the difference between the filtered data (from 5Hz to 15Hz) and their Hilbert transform.

[11] To eliminate spikes or glitches we decimate the data by keeping the median of 1000 consecutive points, corresponding to 10 seconds. This leads to the seismic intensity estimate, I, that we will use from now.

[12] The last step of the analysis is a median filter applied on I using a sliding window of given duration Δt. The

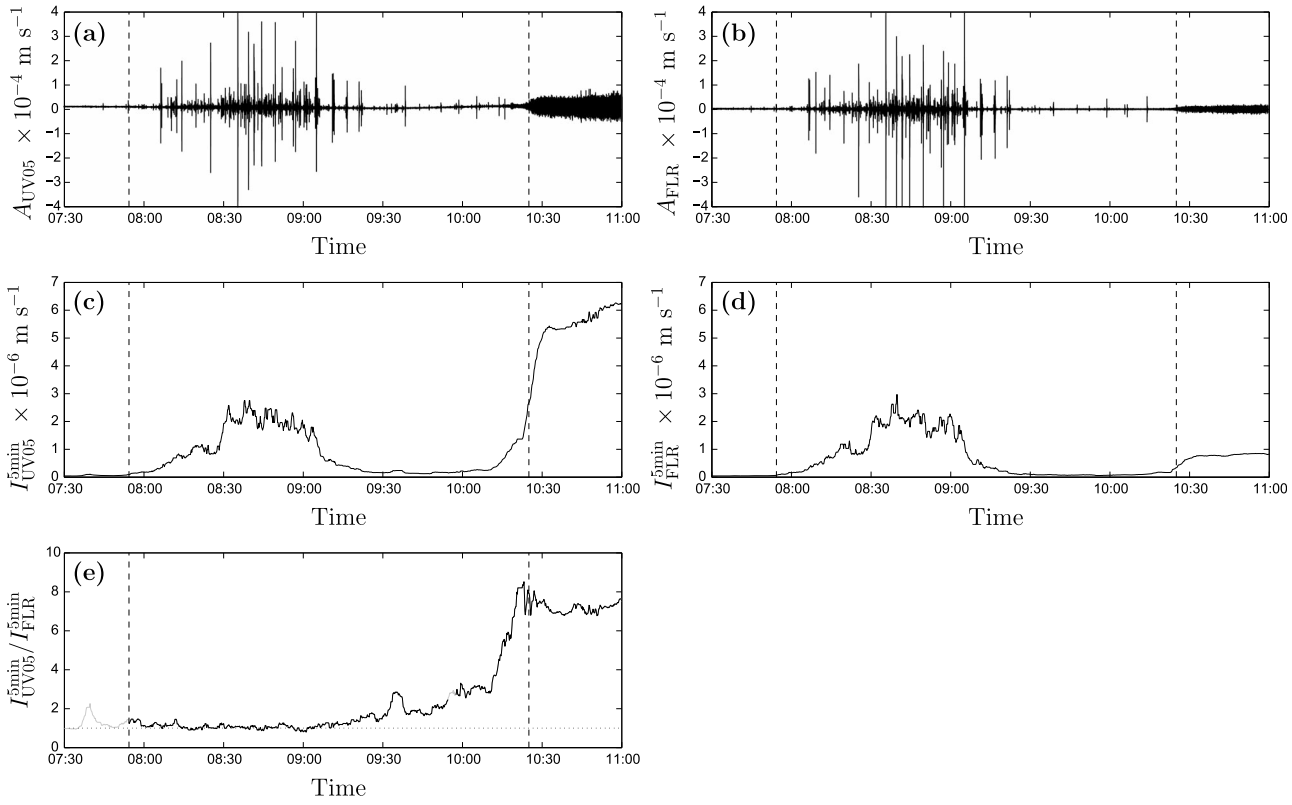

Figure 2. Example of data processing. (a and b) The raw ground velocity at stations UV05 and FLR respectively. (c and d) The seismic intensities, see section 3 for further details. (e) The ratio between I^{5min}_{UV05} and I^{5min}_{FLR}. Vertical dashed lines represent the beginning of the seismic swarm (07:54 AM) and the onset of the eruption (10:25 AM).

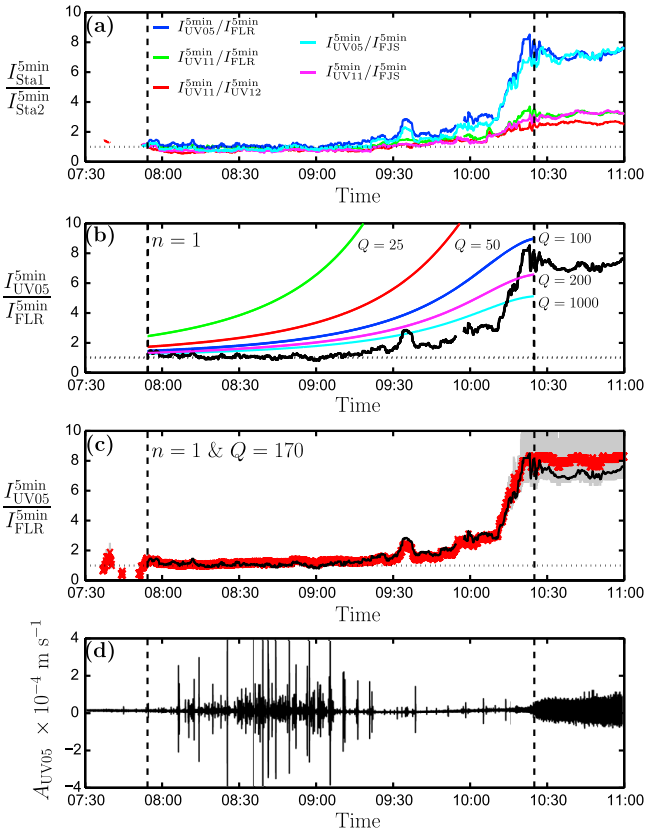

Figure 3. (a) Seismic intensity ratio for five different station pairs (Δt = 5 min). (b) Comparison of real and synthetic ratios for station pair UV05, FLR using different quality factors and considering body wave attenuation (n = 1). The synthetic curves are calculated for a source migrating at constant vertical velocity from sea level at 07:54 AM to the vent at 10:25 AM. (c) The red cross and vertical grey lines correspond to the calculated ratio based on the inversion result (n = 1 and Q = 170) and corresponding error calculated using neighbor grid nodes (see section 5 for detail). (d) Raw ground velocity at station UV05 for timing comparison. Vertical dashed lines represent the beginning of the seismic swarm (07:54 AM) and the onset of the eruption (10:25 AM).

second median filter is used to diminish the importance of bigger earthquakes.

[13] The nomenclature used is:

$$I^{\Delta t}_{\mathrm{Sta}}, \tag{4}$$

where Sta refers to the station's name. Figures 2c and 2d represent the results of this data processing for Δt = 5min.

[14] To highlight relative changes of intensity between different stations we plot the ratio $I^{\Delta t}_{\mathrm{Sta}_1}/I^{\Delta t}_{\mathrm{Sta}_2}$ (one example is shown in Figure 2e).

4. Results

[15] Ratios for 5 different pairs of stations are shown Figure 3a. It is important to note that since this method relies on the seismic emissions from the dike's tip, we only show results corresponding to periods when signal intensities $I^{\Delta t}_{Sta}$ are at least twice the background seismic noise intensity level that precedes the seismic swarm.

[16] We then compare the observed intensity ratio for the station pair UV05-FLR with synthetic ones (Figure 3b) obtained for a theoretical vertical pathway beneath the eruptive vent and a constant propagation velocity from sea level (0 meters a.s.l at 07:54 AM) to the surface (2500 m at 10:25 AM), and using the results of the inversion (Figure 3c, details section 5).

[17] The intensity ratios are calculated using equation (3) for different value for the quality factor (Q) and assuming body wave attenuation. An interesting point is the behaviour of the theoretical curve that presents an apparent acceleration since the migration is set to be at constant speed.

[18] In Figure 3, the beginning of the seismic swarm (07:54 to 09:00 AM) shows a high level of seismicity with intensity ratios close to unity and with no significant variations which reveals that the magma has not yet started its migration. In the later part of the seismic swarm (09:00 AM to 10:25 AM) seismic activity strongly decreases and intensity ratios show strong variations that can be interpreted as a fast migration of the magma in the shallow part of the edifice. As shown by equation (3) any time change in the ratio is therefore due to a migration of the source of the seismicity. This migration presents some variability with a phase of arrest around 10:00 AM. Models with constant propagation velocities do not explain the temporal change of the intensity ratio and show that simple migration is not likely to occur in this case.

[19] Regarding the ratios presented in Figure 3a, the slope change at 10:09 AM could be due to a change in the direction of the propagation from vertical to horizontal toward station UV05. This highlights the need to develop an inverse problem to extract the position of the propagating front from all the possible intensity ratios.

5. Inverse Problem

[20] In order to image magma propagation at depth, we seek the position within a grid that best explains the intensity ratios from all possible pairs of stations. We process a simple inverse problem in which we compute all the theoretical intensity ratios on each point of the grid defined as follows: Easting from 362 km to 370 km every 100 m, Northing from 7647 km to 7653 km every 100 m and depth from −0.5 km to 2.5 km above see level every 50 m. The range of depth is defined from the deepest events located at the beginning of the seismic swarm, to the top of the edifice. Since the size of the active propagating front (about 100 m) is smaller than the source to receiver distance, we may consider a single source of isotropic radiated seismicity (composed of numerous events presenting random orientation). The inversion is done assuming a homogeneous and isotropic medium. Parameters used for the attenuation law are n = 1, Q = 170, f = 10 Hz and β = 1 km s^{-1}. This set of parameters, corresponds to seismic intensities dominated by body waves, allowing inversion of the depth.

[21] The 3-dimensional misfit used is the following:

$$\chi = \sqrt{\sum_i \sum_{j>i} \left(\frac{I^{\Delta t}_{\mathrm{Sta}_i}}{I^{\Delta t}_{\mathrm{Sta}_j}}\bigg|^{\mathrm{calculated}} - \frac{I^{\Delta t}_{\mathrm{Sta}_i}}{I^{\Delta t}_{\mathrm{Sta}_j}}\bigg|^{\mathrm{measured}} \right)^2}. \tag{5}$$

The misfit is calculated at each time-step using the data and equation (3). The results are shown in Figure 4. Corresponding calculated seismic ratio is shown, for one pair of stations, Figure 3c, with error calculated using locations corresponding to grid points in the direct neighborhood of the best location.

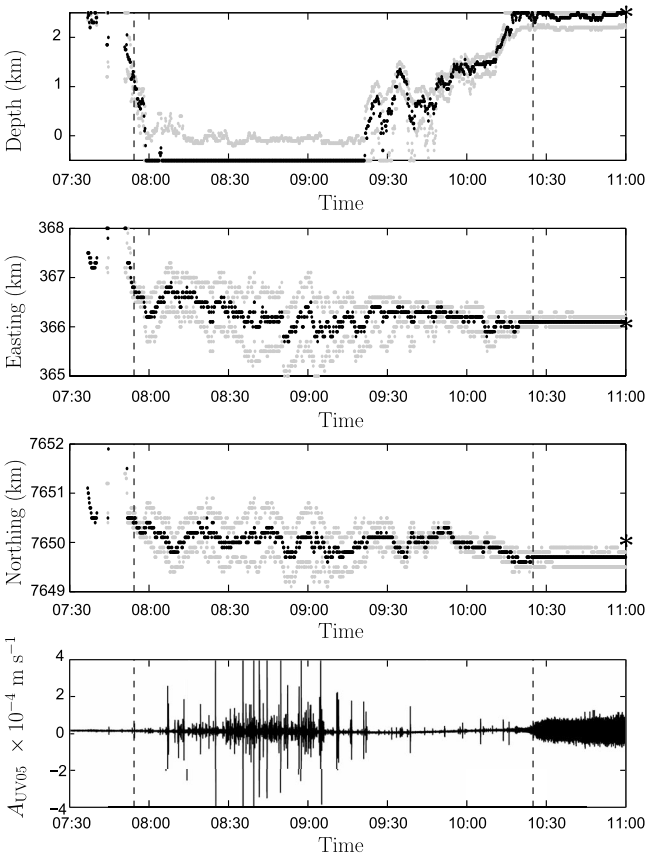

Figure 4. Inversion results for $n = 1$, $Q = 170$, $f = 10$ Hz and $\beta = 1$ km s^{-1}. The top three panels show the results of the inversion in terms of depth (above sea level), Easting and Northing. For each component, the black curve represents the best position of the minimum misfit and both grey curves represent the minimum and maximum extension of a volume including misfit values inferior to 10% of the minimum misfit (see auxiliary material for an animation of the migrating 10% ellipsoid above the minimum misfit, and 3-D representation of the misfit). The bottom panel represents the raw ground velocity at station UV05 for timing comparison. Vertical dashed lines represent the beginning of the seismic swarm (07:54 AM) and the onset of the eruption (10:25 AM). The black stars show the location of the eruptive fissure.

[22] During the period of high seismic activity, locations are saturated at sea level which is consistent with commonly observed seismicity on PdF volcano and the location of single events at the beginning of seismic swarms. As already observed in Figure 3, the inversion results show a phase of arrest around 10:00 AM.

[23] The method had been tested and validated to locate the volcanic tremor (dominated by surface waves) with $n = 0.5$ and $Q = 50$ as done by *Ferrazzini et al.* [1991], *Battaglia and Aki* [2003], and *Battaglia et al.* [2005b]. Other subsurface activity had been successfully tracked using surface waves [*Gottschämmer and Surono*, 2000; *Jolly et al.*, 2002].

6. Discussions and Conclusions

[24] The proposed analysis will find a limitation when the source of the seismicity is far from all the stations. In that case, the relative difference in the source-receiver paths are negligible and all possible intensity ratios will be close to one. This also implies, for future inversion of swarm migration using intensity ratios, that the error in the position will be a function of the position itself: the greater the source-receiver distance, the greater the error will be. Another source of error will be the presence of two distinct sources of sustained seismic emission of similar energy like volcanic tremor [*Battaglia et al.*, 2005b, Appendix A]. Nevertheless, when following magma migration the potential other sources of seismicity are rock falls or distant earthquakes. They will only affect the analysis if they are 2 times longer than the time-windows used for the median filter and of significant energy. Even then the perturbation will affect only a few minutes over the few hours that the migration lasted.

[25] In terms of the dynamics of magma propagation, the results clearly show that the upward migration started between 9:00 AM and 9:30 AM. Combining intensity ratios (Figure 3) and the results of the inversion (Figure 4) we can infer that the migration initiates at 9:00 AM with clear migration toward the surface at 9:25 AM, which corresponds to about one hour after the beginning of the seismic swarm (see the auxiliary material for Animation S1).[1] At smaller scale the upward propagation does not occur at constant velocity but presents phases of rapid propagation and phases of arrest or with a strong decrease of velocity, as stipulated by *Taisne and Jaupart* [2009] and *Taisne and Tait* [2011] for complex magma propagation.

[26] This simple analysis can be easily applied to real time monitoring of magma migration and gives an opportunity to extract information on the dynamics of magma propagation.

[27] In future studies a more complete inverse problem should be done (with inversion of n and Q as well as location) including scattering effect that could be dominant in active volcanos [*Wegler*, 2003; *Friedrich and Wegler*, 2005; *Parsiegla and Wegler*, 2008].

[28] **Acknowledgments.** The data used for the analysis was collected by the Institut de Physique du Globe de Paris, Observatoire Volcanologique du Piton de la Fournaise (IPGP/OVPF) and the Laboratoire de Géophysique Interne et Tectonophysique (LGIT) within the framework of ANR_08_RISK_011/UnderVolc project. The sensors are properties of the réseau sismologique mobile Français, Sismob (INSU-CNRS). We are grateful to Daniel Clarke and Andy Norris for fruitful comments about the manuscript. Careful comments and criticisms by 2 anonymous reviewers led to substantial improvement. This work has been supported by ANR (France) under contracts 05-CATT-010-01 (PRECORSIS), ANR-06-CEXC-005 (COHERSIS), ANR-08-RISK-011 (UNDERVOLC) and by a FP7 European Research Council advanced grant 227507 (WHISPER). This is IPGP contribution 3121. E. Calais thanks Paul Segall and an anonymous reviewer.

References

Aki, K., and V. Ferrazzini (2000), Seismic monitoring and modeling of an active volcano for prediction, *J. Geophys. Res.*, *105*, 16,617–16,640, doi:10.1029/2000JB900033.

Aoki, Y., P. Segall, T. Kato, P. Cervelli, and S. Shimada (1999), Imaging magma transport during the 1997 seismic swarm off the Izu Peninsula, Japan, *Science*, *286*, 927–930.

Battaglia, J., and K. Aki (2003), Location of seismic events and eruptive fissures on the Piton de la Fournaise volcano using seismic amplitudes, *J. Geophys. Res.*, *108*(B8), 2364, doi:10.1029/2002JB002193.

[1] Auxiliary materials are available in the HTML. doi:10.1029/2010GL046068.

Battaglia, J., V. Ferrazzini, T. Staudacher, K. Aki, and J.-L. Cheminée (2005a), Pre-eruptive migration of earthquakes at the Piton de la Fournaise volcano (Réunion Island), *Geophys. J. Int.*, *161*, 549–558.

Battaglia, J., K. Aki, and V. Ferrazzini (2005b), Location of tremor sources and estimation of lava output using tremor source amplitude on the Piton de la Fournaise volcano: 1. Location of tremor sources, *J. Volcanol. Geotherm. Res.*, *147*, 268–290, doi:10.1016/j.jvolgeores.2005.04.005.

Ferrazzini, V., K. Aki, and B. Chouet (1991), Characteristics of seismic waves composing Hawaiian volcanic tremor and gas-piston events observed by a near-source array, *J. Geophys. Res.*, *96*, 6199–6209, doi:10.1029/90JB02781.

Friedrich, C., and U. Wegler (2005), Localization of seismic coda at Merapi volcano (Indonesia), *Geophys. Res. Lett.*, *32*, L14312, doi:10.1029/2005GL023111.

Gottschämmer, E., and I. Surono (2000), Locating tremor and shock sources recorded at Bromo Volcano, *J. Volcanol. Geotherm. Res.*, *101*, 199–209, doi:10.1016/S0377-0273(00)00171-2.

Hayashi, Y., and Y. Morita (2003), An image of magma intrusion process inferred from precise hypocentral migration of the earthquake swarm east of the Izu Peninsula, *Geophys. J. Int.*, *153*, 159–174.

Jolly, A., G. Thompson, and G. Norton (2002), Locating pyroclastic flows on Soufriere Hills Volcano, Montserrat, West Indies, using amplitude signals from high dynamic range instruments, *J. Volcanol. Geotherm. Res.*, *118*, 299–317, doi:10.1016/S0377-0273(02)00299-8.

Parsiegla, N., and U. Wegler (2008), Modelling of seismic energy transport at volcanoes with real topography and complex propagation medium, *J. Volcanol. Geotherm. Res.*, *171*, 229–236, doi:10.1016/j.jvolgeores.2007.12.001.

Rubin, A. M., and D. Gillard (1998), Dike-induced earthquakes: Theoretical considerations, *J. Geophys. Res.*, *103*, 10,017–10,030.

Taisne, B., and C. Jaupart (2009), Dike propagation through layered rocks, *J. Geophys. Res.*, *114*, B09203, doi:10.1029/2008JB006228.

Taisne, B., and S. Tait (2011), Effect of solidification on a propagating dike, *J. Geophys. Res.*, *116*, B01206, doi:10.1029/2009JB007058.

Wegler, U. (2003), Analysis of multiple scattering at Vesuvius volcano, Italy, using data of the TomoVes active seismic experiment, *J. Volcanol. Geotherm. Res.*, *128*, 45–63, doi:10.1016/S0377-0273(03)00246-4.

F. Brenguier and V. Ferrazzini, Observatoire Volcanologique du Piton de la Fournaise, UMR 7154, Institut de Physique du Globe de Paris, Sorbonne Paris Cité, CNRS, 14RN3 - Km 27, 97418 La Plaine des Cafres, La Réunion.

N. M. Shapiro and B. Taisne, Department of Seismology, UMR 7154 Institut de Physique du Globe de Paris, Sorbonne Paris Cité, CNRS, 1 rue Jussieu, F-75238 Paris, CEDEX 5, France. (taisne@ipgp.fr)